Nanoporous Waveguide Sensor with Optimized Nanoarchitectures for Highly Sensitive Label-Free Biosensing

Kazuhiro Hotta,[†] Akira Yamaguchi,[‡] and Norio Teramae[†,*]

[†]Department of Chemistry, Graduate School of Science, Tohoku University, Aoba-ku, Sendai 980-8578, Japan, and [‡]College of Science and Frontier Research Center for Applied Atomic Sciences, Ibaraki University, 2-1-1 Bunkyo, Mito, Ibaraki 310-8512, Japan

Development of label-free biosensors with high sensitivity and specificity has become increasingly important for high-throughput clinical analysis and drug discovery[1,2] since labeling of analytes with fluorescent or electroactive molecules may significantly interfere with the original function of biomolecules and it also requires laborious and costly modifications of analytes. During the past decade, novel label-free biosensors have been steadily studied from the viewpoint of benefits of the nanotechnologies, and a variety of biosensors based on many different types of nanostructures, such as nanowires,[3,4] nanopores,[5,6] nanogaps,[7] nanopipettes,[8] and nanotubes,[9,10] have been developed to improve the sensor performance. Nanoporous metal-oxide membranes that have uniform pore structures with narrow pore size distribution have been expected to serve as a platform for label-free optical biosensors because the electromagnetic field of the probing light can efficiently overlap with the membrane layer composed of nanopores in which target molecules are entrapped.[11−21] In addition, the large internal surface area and the molecular sieve effect of nanopores are considerable advantages for enhancing the sensitivity and selectivity of the biosensors based on nanoporous metal-oxide membranes.

Optical biosensors based on nanoporous metal-oxide membranes are a kind of refractometric sensor; changes in the refractive index (RI) of a membrane accompanied by adsorption of an analyte into the nanopores have been monitored by optical interferometry[11−14] or optical waveguide spectroscopy.[15−21] In general, the sensitivity of refractometric sensors is not so high compared to fluorometric sensors because the changes in the RI induced by molecular adsorption are generally small. Accordingly, making a significant improvement of the sensor response is the key issue to develop optical biosensors based on the nanoporous metal-oxide

ABSTRACT Label-free optical biosensors have attracted much attention, and nanoporous metal-oxide membranes with uniform pore structure and diameter are promising candidates for platforms of label-free optical biosensors. However, development of such sensors with high sensitivity still remains challenging. In this paper, we report on the remarkably enhanced sensitivity of a label-free nanoporous optical waveguide (NPWG) sensor composed of a porous anodic alumina (PAA) waveguiding film and an aluminum cladding film. The enhanced sensitivity was achieved by engineering nanostructures and tuning optical properties of the PAA film. Careful tuning of the porosity, pore density, thickness, and refractive index of the PAA film could significantly improve the sensitivity of the NPWG sensor toward adsorption of bovine serum albumin (BSA) onto the PAA surface, and the optimized sensor responded to the adsorption of BSA with an extraordinarily large red shift (>300 nm) of a waveguide mode due to the large adsorption capacity of the PAA film and the inherently high sensitivity of the waveguide mode. The Fresnel calculations suggested that the potential sensitivity of the NPWG sensor was much higher than that of the conventional surface plasmon resonance (SPR) sensors.
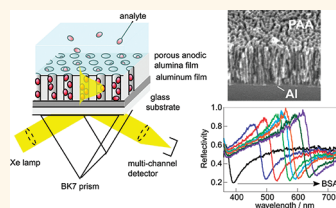
KEYWORDS: porous anodic alumina · nanopores · label-free · biosensing · optical waveguide sensor

membranes. Herein, we report on the remarkably enhanced sensitivity of a label-free nanoporous optical waveguide (NPWG) sensor composed of a porous anodic alumina (PAA) waveguiding film and an aluminum (Al) cladding film deposited on a glass substrate (Figure 1a).[19,20] The enhanced sensitivity was achieved by engineering nanostructures and tuning optical properties of the PAA film.

Among the components of the NPWG sensor, a key feature of the PAA film is that its well-defined nanostructure can be easily and reproducibly fabricated by simple anodization of an Al film in an acidic electrolyte solution.[22] The PAA membrane has a packed array of cylindrical nanopores, and the pore structure as well as the RI of the PAA membrane can be discretionarily tuned

* Address correspondence to
teramae@mail.tains.tohoku.ac.jp.
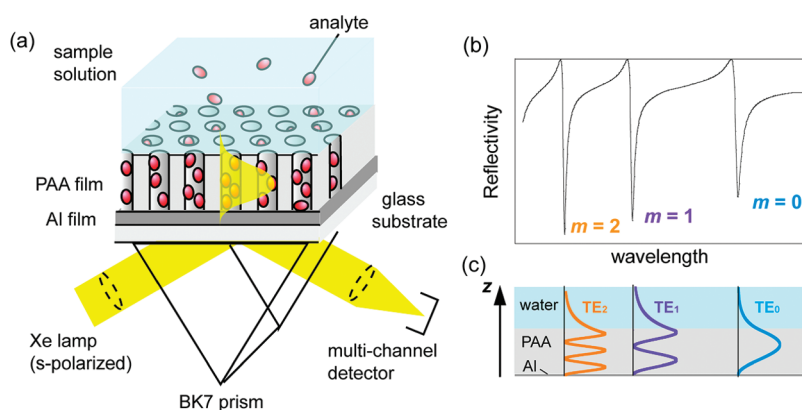
Figure 1. (a) Schematic illustration of the NPWG sensor based on the PAA/Al multilayer film. (b) Typical reflection spectrum of the PAA/Al multilayer film measured in the Kretschmann configuration and (c) electric field distributions of the TE waveguide modes with different mode orders (*m*).

by controlling the anodizing conditions and post-synthesized pore widening conditions in an etchant (typically phosphoric acid solution).[23] In the NPWG sensor, changes in reflection spectra of the PAA/Al multilayer films are measured in the Kretschmann configuration (Figure 1a), similarly to the conventional surface plasmon resonance (SPR) sensor. As schematically illustrated in Figure 1b,c, various orders of waveguide modes characterized by different electric field distributions can be excited at the PAA/Al film by irradiating the PAA/Al film with polarized white light at a certain angle of incidence, which is recognized as the appearance of sharp dips (waveguide coupling dips) in a reflection spectrum.[24] In contrast to the SPR sensor that shows a steep electric field decay from the metal film,[24] the NPWG sensor has a wide electric field distribution at a deep region from the Al film. Wavelength of the dip for a certain order (*m*) of the waveguide mode depends on the incident angle and polarization of incident light, and it also depends on the thickness and the RI of the PAA film. Although p-polarized incident light can also be used to excite the transverse magnetic (TM) modes in the waveguide, we examined the NPWG sensor focusing on the transverse electric (TE) modes excited by s-polarized light because the TE modes are known to exhibit higher sensitivity than TM modes.[25]

The wavelength position of a waveguide coupling dip red shifts by increasing the RI of the PAA film (n_{PAA}) accompanied by adsorption of an analyte to the film, and the shift of the waveguide coupling dip ($\Delta\lambda_{OWG}$) can be approximately expressed as follows:[20]

$$\Delta\lambda_{OWG} = aq_{BSA} \qquad (1)$$

where *a* is the proportional constant determined mainly by both the RI of the PAA waveguiding film and the order of the waveguide mode *m*, and q_{BSA} is the total amount of an adsorbed analyte. Thus, the response of the NPWG sensor ($\Delta\lambda_{OWG}$) provides quantitative information on the adsorbed analyte.
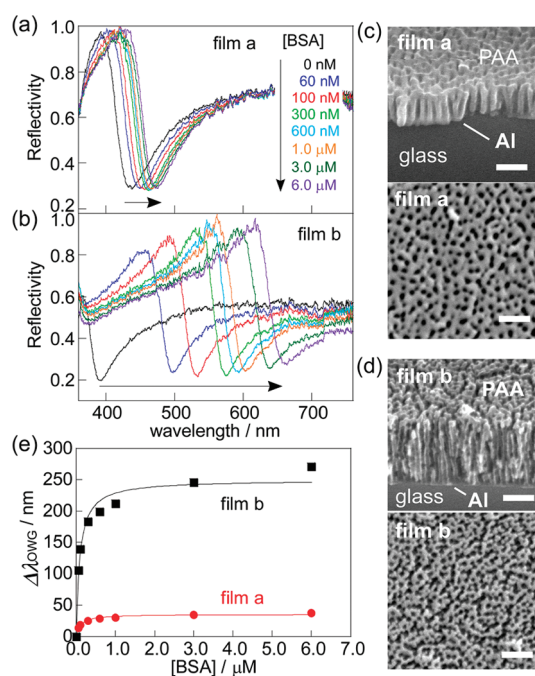
Figure 2. (a,b) Reflection spectra of the PAA/Al multilayer films measured in contact with different concentrations of BSA solutions. Each spectrum was taken after the adsorption of BSA reached equilibrium. The cross-sectional and top SEM views of the PAA films are shown in (c) and (d) that were, respectively, used to measure (a) and (b). The scale bars correspond to 200 nm. (e) Shift of the coupling dip *vs* the concentration of BSA in the solution phase. The solid line is the best fit curve to the Langmuir adsorption isotherm for each film.

To attain the enhanced response of the NPWG sensor, it is necessary to increase q_{BSA} as well as the sensitivity factor of the proportional constant *a*. Herein, we present a highly sensitive NPWG sensor by fabricating a PAA/Al multilayer film that has a large pore density, porosity, large film thickness, and low RI of the PAA layer. The NPWG sensor with an optimized PAA waveguiding film exhibits remarkably larger sensor response compared to other label-free optical sensors.

RESULTS AND DISCUSSION

The response of the NPWG sensor was examined by monitoring the changes in the reflection spectra of the PAA/Al multilayer film for adsorption of bovine serum albumin (BSA) by the PAA waveguiding film. BSA is well-known to adsorb onto the alumina surface to form a monolayer.[26] BSA is a globular protein with dimensions of $4 \times 4 \times 14$ nm^3 that make it small enough to penetrate into the PAA pores of several tens to a hundred nanometers in diameter.[27]

Figure 2a,b shows typical sensor responses for adsorption of BSA obtained by the NPWG sensors with different PAA films (designated as films **a** and **b**, respectively). First, both films **a** and **b** were prepared by deposition of Al on glass substrates using vacuum evaporation and had thicknesses of 180 and 500 nm, respectively. Then the PAA layer was formed by partial anodization of the Al layer. Film **a** was obtained by anodization under a constant potential of 30 V followed by PAA pore widening in a 10 wt % phosphoric acid solution for 10 min. Film **b** was similarly fabricated using an anodization potential of 15 V and PAA pore widening time of 30 min. The structural parameters of films **a** and **b** were evaluated by SEM images (Figure 2c,d) and are summarized in Table 1 (for evaluation procedures, see the Experimental Section).

In the measurements of the sensor response, the single transverse electric (TE$_0$) mode was excited in the PAA/Al films, and sharp dips are recognized in their reflection spectra, as shown in Figure 2a,b. The dip undergoes a red shift as the concentration of BSA increases. A plot of $\Delta\lambda_{OWG}$ against the BSA concentration in the solution phase represents the adsorption isotherm of BSA. The experimental points (Figure 2e) are well fitted to the Langmuir adsorption equation, and the adsorption constant and maximum shift value ($\Delta\lambda_{OWG}^{max}$) are estimated as 0.96×10^7 M^{-1} and 35.7 nm for film **a** and 1.07×10^7 M^{-1} and 250 nm for film **b**, respectively. The sensor response ($\Delta\lambda_{OWG}$) obtained for film **b** is about 7 times larger than that for film **a**, while the adsorption constants are almost the same for both films. The larger sensor response for film **b** is ascribed to its larger sensitivity factor (a) and q_{BSA} (eq 1) compared to those for film **a**.

To investigate in detail the relationship between the sensor response and the structural parameters of the PAA waveguiding film, we systematically tuned the pore density and the porosity of the PAA film by changing the anodization potential and pore widening time in an etchant, respectively (see Experimental Section). Figure 3a shows the SEM top views of the PAA films with different pore densities and porosities. The films **1**−**3** were fabricated using an anodization potential of 10 V, and the resultant pore density was estimated as 7.6×10^{10} cm^{-2}. The films **4**−**6** and **7**−**9** were obtained by anodizing Al films at 20 and 30 V,

**TABLE 1. Structural Parameters of the PAA Films a and b Used for the Optical Waveguide Measurements**[a]

sample	thickness	pore diameter	pore density	porosity
film **a**	220 nm	39 nm	2.8×10^{10} cm^{-2}	34%
film **b**	670 nm	33 nm	5.0×10^{10} cm^{-2}	45%

[a] Parameters of the PAA films were determined by analyzing the SEM images with the image analyzing software as described in the Experimental Section.

respectively, and the pore densities were, respectively, 3.6×10^{10} and 1.4×10^{10} cm^{-2}. The thickness of the PAA film was adjusted to around 500 nm for all of the prepared films by setting the initial thickness of the vapor-deposited Al film as 370 nm. The responses ($\Delta\lambda_{OWG}$) of the NPWG sensors with different PAA films were examined for the adsorption of 1 μM BSA, and the results are shown in Figure 3b, where the sensor response is plotted against the porosity of the PAA film. In the measurements, the incident angle of light was adjusted for each film so that the waveguide modes were excited in the wavelength range of the optical detector (360−760 nm) (see Supporting Information). Here the concentration of BSA was set as 1 μM because saturated adsorption is recognized for 1 μM BSA irrespective of the structures of the PAA films (Figure 2e). As shown in Figure 3b, the order of the waveguide modes excited at the PAA/Al waveguides depends on the porosity and pore density of the PAA films; the lower order mode is excited in the films with larger porosity and larger pore density. In several films, two different orders of the waveguide modes can be excited by changing the incident angle (TE$_0$ and TE$_1$ for films **2**, **5**, and **8** and TE$_1$ and TE$_2$ for film **7**) while only one mode can be excited in the other films (TE$_0$ for films **3**, **6**, and **9** and TE$_1$ for films **1** and **4**).

From Figure 3b, it can be immediately seen that the TE$_0$ waveguide mode shows higher sensor response ($\Delta\lambda_{OWG}$) compared to the TE$_1$ and TE$_2$ modes and that the sensor response is higher for the films with larger porosity and pore density when compared for the same order of the waveguide mode. The increased sensor response for the films with large porosity and pore densities can be ascribed to the increased amount of adsorbed BSA (q_{BSA}) because of the high surface area of the films. On the other hand, the increased sensor response for the lower order waveguide mode is ascribed to the increase in the sensitivity factor a in eq 1. The $\Delta\lambda_{OWG}$ accompanied by the increase in the RI of the PAA film (Δn_{PAA}) was simulated by the Fresnel calculations for different refractive indices of the PAA films with a thickness of 500 nm, and results are plotted in Figure 4. As clearly seen there, the waveguide modes are more sensitive to Δn_{PAA} when the mode order and the RI of the PAA film are low.

Typical dispersion of the refractive indices of the PAA waveguiding films is shown in Figure 5, which represents the refractive indices estimated for the PAA films
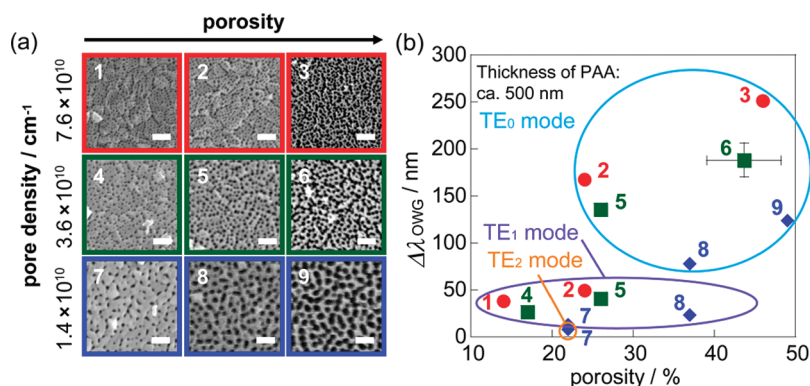
Figure 3. (a) SEM top views of the PAA films with different pore densities and porosities. The scale bars correspond to 200 nm. (b) Shifts of the waveguide coupling dip induced by adsorption of BSA (1 μM) to the PAA/Al multilayer films. Numbers given for each point correspond to the numbers given in (a). The thickness of the PAA films was around 500 nm. The error bars represent the standard deviation (3σ) observed for three different PAA/Al films fabricated under the same conditions (for structural parameters of PAA/Al films, see Table S1 in the Supporting Information).
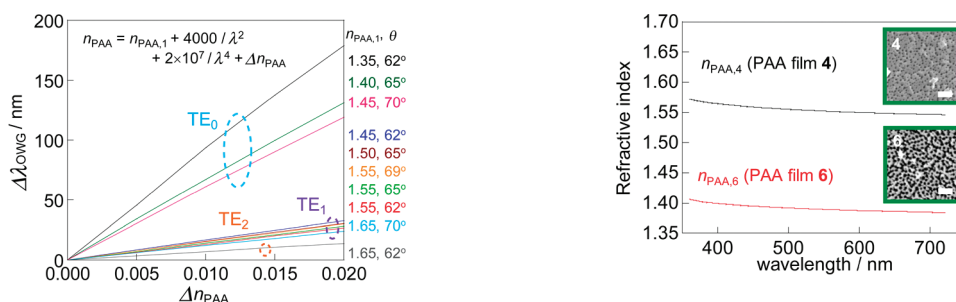

Figure 4. Shift of the waveguide modes ($\Delta\lambda_{OWG}$) simulated by the Fresnel calculations for various refractive indices of the PAA films (n_{PAA}) and incident angles of light (θ). The refractive index of the PAA film was assumed to be wavelength (λ)-dependent, i.e., $n_{PAA} = n_{PAA,1} + 4000/\lambda^2 + 2 \times 10^7/\lambda^4$, and the $n_{PAA,1}$ value is given in the figure for each simulation. The incident angle of light was chosen to excite the waveguide modes in the measurable wavelength range of the optical setup.

4 and **6** in Figure 3a by analyzing reflection spectra of the PAA/Al films with the Fresnel calculations (see Supporting Information for details). The RI decreases from $n_{PAA} \approx 1.55$ (film **4**) to $n_{PAA} \approx 1.40$ (film **6**) as a consequence of the porosity increase. The remarkable decrease in the RI results in the excitation of the lower order waveguide mode in the PAA/Al waveguiding film, which enhanced the inherent sensitivity of the sensor (a) in accordance with the simulated results shown in Figure 4.

We also investigated the dependence of $\Delta\lambda_{OWG}$ observed for adsorption of 1 μM BSA on the thickness of the PAA films whose porosity was adjusted to 40—50% to excite the TE$_0$ mode. The PAA films with thicknesses of around 320, 500, and 670 nm were obtained by anodizing the Al films with thicknesses of 240, 370, and 500 nm, respectively. As shown in Figure 6, the PAA films having the same pore density have almost linear dependence of $\Delta\lambda_{OWG}$ on the thickness of the PAA film, and the larger $\Delta\lambda_{OWG}$ is recognized for films with larger pore density, which can be simply explained by the increase in q_{BSA}.


Figure 5. Changes in the refractive index of the PAA film upon pore widening of the PAA film. The black and red curves, respectively, represent the refractive indices of the PAA films 4 and 6 in Figure 3a, which were estimated from reflection spectrum of each film by using the Fresnel calculations.
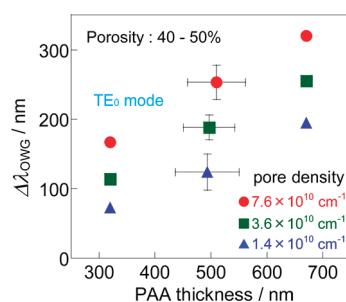
Figure 6. Shifts of the waveguide coupling dip induced by adsorption of BSA at the PAA/Al multilayer films with different PAA thicknesses and pore densities. The error bars represent the standard deviation (3σ) observed for three different PAA/Al films fabricated under the same conditions (for structural parameters of PAA/Al films, see Table S2 in the Supporting Information).

From the experimental results, we can conclude that the improvement in a as well as q_{BSA} by tuning the nanoarchitectures of the PAA film is essential in developing an optimized NPWG sensor with high sensitivity. The potentially high sensitivity is attained by using the TE$_0$ mode excited in a thick and low RI PAA film with large pore density and porosity. Here, we note that the amount of the coupling dip shift ($\Delta\lambda_{OWG}$) obtained by
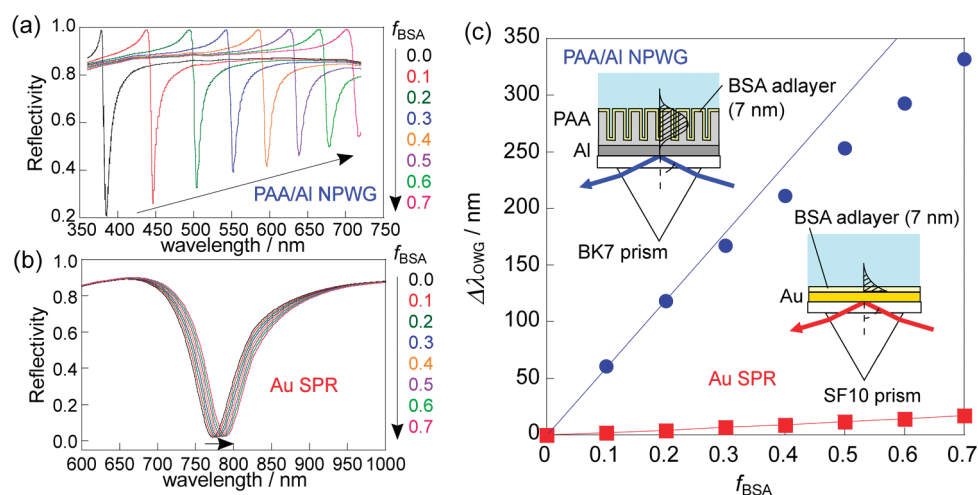
Figure 7. Changes in reflection spectra simulated by the Fresnel calculations depending on the surface coverage of BSA molecules (f_{BSA}) adsorbed by (a) the PAA film (PAA/Al/BK7 NPWG sensor) and (b) the Au surface (Au/SF10 SPR sensor). (c) Shifts of the waveguide coupling and SPR dips vs f_{BSA}.

the optimized NPWG sensor is more than 300 nm (see Figure 6), and this value is remarkably larger than the wavelength shifts reported for other refractometric biosensors based on nanoporous membranes. For example, the porous silicon microcavity developed by Ouyang et al.[13] showed a 17 nm shift of the resonance dip for binding of streptavidin to the biotin-immobilized sensor surface from a 1 mg/mL (ca. 17 μM) streptavidin solution. The nanoporous leaky waveguide sensor comprised a nanoporous TiO$_2$ waveguide, and a Au cladding film reported by Qi et al.[16] responded to adsorption of myoglobin from 5 μM solution, showing a 6.5 nm red shift of the waveguide coupling mode. Of course, the adsorption constant will be different for a different set of proteins and surfaces, and thus, we cannot simply compare the amount of sensor response; however, the extraordinarily large red shift (>300 nm) obtained for the present NPWG sensor with the optimized PAA waveguiding film indicates the high applicability of the NPWG sensor for label-free biosensing.

Finally, we compared the sensor response of the NPWG sensor with that of a conventional SPR sensor which has been widely used as a standard for label-free optical biosensing. The comparison was performed by simulating the sensor response for the adsorption of BSA based on the Fresnel calculations. In the simulation, changes in reflection spectra of the PAA/Al film were calculated as a function of coverage of BSA molecules adsorbed at the internal and the external surfaces of the PAA film, assuming homogeneous adsorption of BSA on the PAA surfaces.[20] The thickness of the BSA monolayer was set as 7 nm according to the experimental results given by Lau et al.,[15] and the RI of the BSA adlayer (n_{ad}) composed of adsorbed BSA and water molecules was calculated by using the Lorentz−Lorenz equation described below:[28]

$$\frac{n_{ad}^2 - 1}{n_{ad}^2 + 2} = \frac{n_{BSA}^2 - 1}{n_{BSA}^2 + 2} f_{BSA} + \frac{n_w^2 - 1}{n_w^2 + 2}(1 - f_{BSA}) \qquad (2)$$

where f_{BSA} is volume fraction of adsorbed BSA in the 7 nm thick adlayer and n_{BSA} and n_w are the refractive indices of a closely packed BSA monolayer and water, respectively. Here, f_{BSA} is equivalent to the coverage of BSA at the PAA surfaces because of the monolayer nature of the BSA adsorption. The RI of the closely packed BSA monolayer ($f_{BSA} = 1$) was assumed to be $n_{BSA} = 1.44 + 5000/\lambda^2$.[29] The parameters of the PAA film were derived from the PAA film which exhibited the largest $\Delta\lambda_{OWG}$ in the experiments and set as follows: thickness, 675 nm; pore density, 7.6 × 10^{10} cm^{-2}; porosity, 46%; average pore diameter, 28 nm. As for SPR, simulation was carried out for BSA adsorbed on a Au film (thickness, 45 nm) attached to an SF10 glass prism. Thickness of the BSA layer was assumed as 7 nm, the same as that for the NPWG sensor. Since, in general, the SPR sensors are more sensitive at a longer wavelength and a wavelength around 800 nm has often been used to develop a sensitive SPR sensor based on the Au film on SF10,[30−32] the calculations were carried out with the initial SPR wavelength at $\lambda_{0SPR} = 780$ nm.

Simulated reflection spectra for the respective NPWG and SPR sensors are shown in Figure 7a,b for the BSA coverage (f_{BSA}) of 0 to 0.7. The wavelength for the dip in the reflection spectrum has a red shift that appears as the BSA coverage increases, and the amount of the shift is significant for NPWG and moderate for SPR, as shown in Figure 7c. The wavelength shift is 20 times larger for NPWG than SPR and is more than 300 nm when $f_{BSA} = 0.7$, which is in good agreement with the observed shift for the NPWG sensor (Figure 6). The saturated adsorption amount of BSA is estimated as 3.43 ng/mm^2 ($f_{BSA} = 1.0$), considering the thickness of the adsorbed BSA layer (7 nm)[15] and the density of BSA (0.49 mg/mm^3).[27] The slope of the linear regression curve shown in Figure 7c is 600 nm ($f_{BSA} < 0.2$) for the NPWG sensor, and the wavelength resolution of the present measurement system is 0.5 nm. Accordingly, if 1.0 nm shift in wavelength can be discriminated, the limit

of detection is estimated as 5.7 pg/mm^2 for NPWG sensing, and the sensitivity will be improved by using instruments with higher wavelength resolutions.

CONCLUSION

The optimization of a NPWG sensor based on a PAA layer on an Al film was done by investigating the relationship between the sensor response and the properties of the PAA waveguiding film. By comparing the sensor responses for adsorption of BSA by the PAA films with different nanoarchitectures, we found that high sensitivity could be achieved using the TE$_0$ waveguide mode excited in a thick and low RI PAA film with large pore density and porosity. The optimized NPWG sensor showed remarkably large sensor response for adsorption of BSA due to the large adsorption capacity of the PAA film (q_{BSA}) as well as

the high inherent sensitivity of the TE$_0$ mode (*a*). Theoretical simulations based on the Fresnel calculations suggested that the potential sensitivity of the NPWG sensor was more than 20-fold higher than that of the conventional SPR sensors. The results obtained here clearly indicate that development of highly sensitive refractometric sensors is possible based on nanoporous membranes by engineering the nanoarchitectures and tuning optical properties of membranes. Although important issues, such as slow diffusion of molecules into nanopores, still remain to be solved in the present NPWG sensor before it can be applied to practical analysis, the extraordinary large red shift of the waveguide mode (>300 nm) obtained for the adsorption of BSA suggests that the NPWG sensor will be an attractive platform for optical label-free biosensing.

EXPERIMENTAL SECTION

Materials. A square cover glass slip (25 × 25 × 0.3 mm; Matsunami Glass Ind., Ltd., Osaka, Japan) was used as a substrate for the PAA/Al multilayer film, and Al wire (99.99%; Nilaco Co., Tokyo Japan) was used for the thermal deposition of Al films. Milli-Q water (Millipore Corp., Bedford, MA) was used for all experiments. All chemical reagents were purchased from Wako Pure Chemical Industries Ltd. (Osaka, Japan) and were used as received.

Fabrication of the PAA/Al Multilayer Film. The PAA/Al multilayer film was fabricated by partial anodization of an Al film deposited on the cover glass substrate.[19] The Al film was thermally evaporated on the glass substrate by using a Ulvac model VPC-1100 vacuum deposition system (ULVAC, Inc., Kanagawa, Japan). The thickness of the Al film during the evaporation was monitored with a quartz crystal thickness meter (model CRTM-6000, ULVAC, Inc., Kanagawa, Japan). The anodization of the Al film was carried out in a 0.3 M oxalic acid solution at 5 °C by applying a constant potential to the Al film. An Al plate was used as a counter electrode, and the solution was vigorously stirred with a magnetic stirrer during anodization. Anodization was continued until the thickness of the remaining Al film was about 14 nm. Around this Al thickness, the transparency of the multilayer film noticeably changes. Thus, the time to stop anodization was determined by monitoring the multilayer film with the naked eye during anodization. This method allowed control of the thickness of the Al film with the precision of about ±2 nm. Then, the resulting PAA/Al multilayer film was washed thoroughly with water and dried under flowing N$_2$ gas. After anodization, the multilayer film was immersed in a 10 wt % phosphoric acid solution for a certain period of time to enlarge the pore diameter and to adjust the porosity of the film. Finally, the film was rinsed with water and dried under flowing N$_2$ gas.

The structural parameters of the PAA film were tuned by fabrication conditions. The thickness of the PAA film was tuned by the deposition time of the Al film. The pore density and porosity was controlled by choosing a suitable anodization potential and time for the pore widening process, respectively.

Optical Waveguide Spectroscopy. The waveguide experiments were carried out by measuring reflection spectra of the PAA/Al multilayer films in the Kretschmann configuration.[21] The multilayer film was attached to a BK7 equilateral glass prism *via* index matching fluid (Cargille; immersion oil no. 16242) and irradiated by collimated white light (ϕ = 1 mm) from a Xe lamp (Hamamatsu Photonics; L8254). The incident light was adjusted to s-polarized light using a polarizer (Sigma Koki Co., Ltd., SPF). Then, the reflected light was detected by a photonic multichannel analyzer (Hamamatsu Photonics; PMA-11). A PDMS flow cell with the cell volume of 2 μL (16 mm × 1.3 mm × 100 μm)

was used to supply sample solutions to the PAA/Al sensor surfaces. The solutions were injected into the flow cell using PFA tubes (0.4 mm i.d.) and a syringe pump. For the BSA adsorption experiments, the BSA solutions containing 5 mM phosphate buffer (pH 4.9) were continuously flowed into the flow cell at a flow rate of 15 μL/min. During the BSA adsorption, the reflection spectra were successively taken at intervals of 30 s until the adsorption of BSA reached equilibrium.

Characterization of the PAA/Al Multilayer Film. Pore density, porosity, and the thickness of the PAA film were determined by a field emission scanning electron microscope (FE-SEM; Hitachi; S-4300). The SEM images were analyzed using "WinRoof" version 5.03 image analyzing software (Mitani Corp. Tokyo, Japan). The thickness and the RI of the PAA film were also determined by measuring reflection spectra of the PAA/Al multilayer films at a series of incident angles and analyzing them by the Fresnel calculations (details are given in Supporting Information).

Fresnel Calculations. The Fresnel calculations were carried out to estimate the structural parameters of the PAA films and to simulate the sensor response of the NPWG sensor. In the calculations, the reflectivity of a four-layer structure composed of the BK7 prism, Al film, PAA film, and surrounding water was calculated based on Fresnel's reflection laws[33] using "Mathematica" version 5.2 software (Wolfram Research, Inc., Champaign, IL). The RI values of all sensor components used in the calculations are given in the Supporting Information.[34−36] To describe the effective RI of the PAA film consisting of an alumina matrix and cylindrical nanopores, we employed the Maxwell−Garnett effective medium approximation (EMA) that considers the cylindrical pore geometry.[37] For s-polarized light that has an electric field component perpendicular to the cylindrical pores, the effective RI of the PAA film (n_{PAA}) was calculated as

$$n_{PAA}^2 = n_{al}^2 + n_{al}^2 \frac{f_{pore}(n_{pore}^2 - n_{al}^2)\beta}{n_{al}^2 - 0.5 f_{pore}(n_{pore}^2 - n_{al}^2)\beta}$$

$$\beta = \frac{2}{n_{pore}^2/n_{al}^2 + 1} \tag{3}$$

where n_{al} and n_{pore} are the RIs of the alumina matrix and the nanopores, respectively, and f_{pore} is the porosity of the PAA film.

The changes in the reflection spectrum of the PAA/Al multilayer film induced by adsorption of BSA to the PAA film were simulated according to the procedures presented in our previous report.[20] In the simulation, BSA was assumed to form a 7 nm thick adlayer at both the internal and external surfaces of the PAA film, and the Fresnel calculations were carried out for

different volume fractions of BSA, that is, different RI values, using the Lorentz−Lorenz equation (eq 2).

Supporting Information Available: Equations and refractive indices used for the Fresnel calculations. Procedures to estimate the thickness and refractive index of the PAA film based on the Fresnel calculations. Structural and process parameters of the PAA films shown in Figures 3 and 6. This material is available free of charge *via* the Internet at http://pubs.acs.org.

REFERENCES AND NOTES

1. Hunt, H. K.; Armani, A. M. Label-Free Biological and Chemical Sensors. *Nanoscale* **2010**, *2*, 1544–1559.
2. Erickson, D.; Mandal, S.; Yang, A. H. J.; Cordovez, B. Nanobiosensors: Optofluidic, Electrical and Mechanical Approaches to Biomolecular Detection at the Nanoscale. *Microfluid. Nanofluid.* **2008**, *4*, 33–52.
3. Cui, Y.; Wei, Q.; Park, H.; Lieber, C. M. Nanowire Nanosensors for Highly Sensitive and Selective Detection of Biological and Chemical Species. *Science* **2001**, *293*, 1289–1292.
4. Gao, Z.; Agarwal, A.; Trigg, A. D.; Singh, N.; Fang, C.; Tung, C.-H.; Fan, Y.; Buddharaju, K. D.; Kong, J. Silicon Nanowire Arrays for Label-Free Detection of DNA. *Anal. Chem.* **2007**, *79*, 3291–3297.
5. Howorka, S.; Cheley, S.; Bayley, H. Sequence-Specific Detection of Individual DNA Strands Using Engineered Nanopores. *Nat. Biotechnol.* **2001**, *19*, 636–639.
6. Sexton, L. T.; Horne, L. P.; Martin, C. R. Developing Synthetic Conical Nanopores for Biosensing Applications. *Mol. BioSyst.* **2007**, *3*, 667–685.
7. Yi, M.; Jeong, K.-H.; Lee, L. P. Theoretical and Experimental Study towards a Nanogap Dielectric Biosensor. *Biosens. Bioelectron.* **2005**, *20*, 1320–1326.
8. Actis, P.; Mak, A. C.; Pourmand, N. Functionalized Nanopipettes: Toward Label-Free, Single Cell Biosensors. *Bioanal. Rev.* **2010**, *1*, 177–185.
9. Star, A.; Tu, E.; Niemann, J.; Gabriel, J.-C. P.; Joiner, C. S.; Valcke, C. Label-Free Detection of DNA Hybridization Using Carbon Nanotube Network Field-Effect Transistors. *Proc. Natl. Acad. Sci. U.S.A.* **2006**, *103*, 921–926.
10. Maehashi, K.; Katsura, T.; Kerman, K.; Takamura, Y.; Matsumoto, K.; Tamiya, E. Label-Free Protein Biosensor Based on Aptamer-Modified Carbon Nanotube Field-Effect Transistors. *Anal. Chem.* **2007**, *79*, 782–787.
11. Lin, V. S.; Motesharei, K.; Dancil, K. P.; Sailor, M. J.; Ghadiri, M. R. A Porous Silicon-Based Optical Interferometric Biosensor. *Science* **1997**, *278*, 840–843.
12. Mun, K.-S.; Alvarez, S. D.; Choi, W.-Y.; Sailor, M. J. A Stable, Label-Free Optical Interferometric Biosensor Based on TiO₂ Nanotube Arrays. *ACS Nano* **2010**, *4*, 2070–2076.
13. Ouyang, H.; Christophersen, M.; Viard, R.; Miller, B. L.; Fauchet, P. M. Macroporous Silicon Microcavities for Macromolecule Detection. *Adv. Funct. Mater.* **2005**, *15*, 1851–1859.
14. Kim, D.-K.; Kerman, K.; Saito, M.; Sathuluri, R. R.; Endo, T.; Yamamura, S.; Kwon, Y.-S.; Tamiya, E. Label-Free DNA Biosensor Based on Localized Surface Plasmon Resonance Coupled with Interferometry. *Anal. Chem.* **2007**, *79*, 1855–1864.
15. Lau, K. H. A.; Tan, L.-S.; Tamada, K.; Sander, M. S.; Knoll, W. Highly Sensitive Detection of Process Occuring inside Nanoporous Anodic Alumina Templates: A Waveguide Optical Study. *J. Phys. Chem. B* **2004**, *108*, 10812–10818.
16. Qi, Z.-M.; Honma, I.; Zhou, H. Nanoporous Leaky Waveguide Based Chemical and Biological Sensors with Broadband Spectroscopy. *Appl. Phys. Lett.* **2007**, *90*, 011102.
17. Awazu, K.; Rockstuhl, C.; Fujimaki, M.; Fukuda, N.; Tominaga, J.; Komatsubara, T.; Ikeda, T.; Ohki, Y. High Sensitive Sensors Made of Perforated Waveguides. *Opt. Express* **2007**, *15*, 2592–2597.
18. Jiao, Y.; Weiss, S. M. Design Parameters and Sensitivity Analysis of Polymer-Cladded Porous Silicon Waveguides for Small Molecule Detection. *Biosens. Bioelectron.* **2010**, *25*, 1535–1538.
19. Yamaguchi, A.; Hotta, K.; Teramae, N. Optical Waveguide Sensor Based on a Porous Anodic Alumina/Aluminum Mutilayer Film. *Anal. Chem.* **2009**, *81*, 105–111.
20. Hotta, K.; Yamaguchi, A.; Teramae, N. Properties of a Metal Clad Waveguide Sensor Based on a Nanoporous-Metal-Oxide/Metal Multilayer Film. *Anal. Chem.* **2010**, *82*, 6066–6073.
21. Yamaguchi, A.; Arafune, H.; Hotta, K.; Itoh, T.; Teramae, N. Adsorption and Desorption Dynamics of Sodium Dodecyl Sulfate at Octadecylsilane Layer on the Pore Surface of a Mesoporous Silica Film Obserbed *in-Situ* by Optical Waveguide Spectroscopy. *Anal. Sci.* **2011**, *27*, 597–603.
22. Thompson, G. E. Porous Anodic Alumina: Fabrication, Characterization and Applications. *Thin Solid Films* **1997**, *297*, 192–201.
23. O'Sullivan, J. P.; Wood, G. C. The Morphology and Mechanism of Formation of Porous Anodic Films on Aluminum. *Proc. R. Soc. London, Ser. A* **1970**, *317*, 511–543.
24. Knoll, W. Interfaces and Thin Films As Seen by Bound Electromagnetic Waves. *Annu. Rev. Phys. Chem.* **1998**, *49*, 569–638.
25. Skivesen, N.; Horvath, R.; Pedersen, H. C. Optimization of Metal-Clad Waveguide Sensors. *Sens. Actuators, B* **2005**, *106*, 668–676.
26. Fukuzaki, S.; Urano, H.; Nagata, K. Adsorption of Bovine Serum Albumin onto Metal Oxide Surfaces. *J. Ferment. Bioeng.* **1996**, *81*, 163–167.
27. Tencer, M.; Charbonneau, R.; Lahoud, N.; Berini, P. AFM Study of BSA Adlayers on Au Stripes. *Appl. Surf. Sci.* **2007**, *253*, 9209–9214.
28. Aspnes, D. E. Optical Properties of Thin Films. *Thin Solid Films* **1982**, *89*, 249–262.
29. McClellan, S. J.; Franses, E. I. Effect of Concentration and Denaturation on Adsorption and Surface Tension of Bovine Serum Albumin. *Colloids Surf. B* **2003**, *28*, 63–75.
30. Goodrich, T. T.; Lee, H. J.; Corn, R. M. Enzymatically Amplified Surface Plasmon Resonance Imaging Method Using RNase H and RNA Microarrays for the Ultrasensitive Detection of Nucleic Acids. *Anal. Chem.* **2004**, *76*, 6173–6178.
31. Nelson, B. P.; Frutos, A. G.; Brockman, J. M.; Corn, R. M. Near-Infrared Surface Plasmon Resonance Measurements of Ultrathin Films. 1. Angle Shift and SPR Imaging Experiments. *Anal. Chem.* **1999**, *71*, 3928–3934.
32. Beusink, J. B.; Lokate, A. M. C.; Besselink, G. A. J.; Pruijn, G. J. M.; Schasfoort, R. B. M. Angle-Scanning SPR Imaging for Detection of Biomolecular Interactions on Microarrays. *Biosens. Bioelectron.* **2008**, *23*, 839–844.
33. Hansen, W. N. Electric Fields Produced by the Propagation of Plane Coherent Electromagnetic Radiation in a Stratified Medium. *J. Opt. Soc. Am.* **1968**, *58*, 380–390.
34. Roth, W. A.; Scheelk, K. In *Landolt Börnstein Tabelen*, Auflage; Springer-Verlag: Berlin, 1931; p 966.
35. Gervais, F. In *Handbook of Optical Constants of Solids II*; Palik, E. D., Ed.; Academic Press, Inc.: Orlando, FL, 1991; pp 761−775.
36. Lynch, D. W.; Hunter, W. R. In *Handbook of Optical Constants of Solids*; Palik, E. D., Ed.; Academic Press, Inc.: Orlando, FL, 1985; pp 286−295.
37. Maldovan, M.; Bockstaller, M. R.; Thomas, E. L.; Carter, W. C. Validation of the Effective-Medium Approximation for the Dielectric Permittivity of Oriented Nanoparticle-Filled Materials: Effective Permittivity for Dielectric Nanoparticles in Multilayer Photonic Composites. *Appl. Phys. B: Laser Opt.* **2003**; *884*, 877−884.
38. Roth, W. A.; Scheelk, K. *Landolt Börnstein Tabelen*, 5 Auflage; Springer-Verlag: Berlin, 1931; p 966.
39. Gervais, F. In *Handbook of Optical Constants of Solids II*; Palik, E. D., Ed.; Academic Press, Inc.: Orlando, FL, 1991; pp 761−775.
40. Lynch, D. W.; Hunter, W. R. In *Handbook of Optical Constants of Solids*; Palik, E. D., Ed.; Academic Press, Inc.: Orlando, FL, 1985; pp 286−295.